Prepared for PHYS736 Final Project

Cosmic-ray detection efficiency in cell phone camera image sensors

Alex Pizzuto[a]

[a] *University of Wisconsin-Madison, Department of Physics, Madison, WI, USA*

E-mail: pizzuto@wisc.edu

Abstract: Although cell phone camera image sensors have the capability to detect ionizing radiation from cosmic rays, the efficiency at which they do so is not understood. We present here a GEANT4 derived simulation of CMOS camera image sensors using the Allpix^2 modular framework. With this simulation, we calculate detector efficiency to various forms of ionizing radiation at different energies, and classify image level observables such as track length and deposited charge for future measurements of the cosmic-ray flux as well as for event by event reconstructions.

Contents

1 Introduction

Commercial and industrial demand for silicon based sensors has led to an exponential growth in instrumented volume of silicon. Although much of the innovation in silicon based technologies can be linked to personal use applications, scientific pursuits such as medical physics, high energy physics, and multimessenger astrophysics have benefited vastly from the recent improvements. However, although many ideas benefit both academic and industrial pursuits, individual devices tend to be unique to the subfield, due to different requirements in specifications.

The Distributed Electronic Cosmic-ray Observatory (DECO) [1] seeks to capitalize on the vast area of instrumented silicon in commercial devices for academic purposes by using camera image sensors to detect ionizing radiation from cosmic-rays. To date, DECO data from all seven continents has led to the identification and classification of various forms of ionizing radiation [2] as well as measurements of detector geometry from the known angular distribution of cosmic-ray muons at sea level [3].

Although DECO can classify forms of ionizing radiation, absolute and independent measurements of the cosmic-ray muon flux require a better understanding of the sensitivity of the detectors. In this work, we present the first simulation of the full detector including beam production, interactions within the silicon pixels, electron-hole transport, and signal digitization, using the Allpix^2 modular simulation framework. Various forms of incident radiation are simulated to search for qualitative and quantitative differences in event signatures, and beams of different energies are used to investigate the dependence of observables on the incident particle energy. In section 2 we review the relevant physics of silicon pixels, and then discuss our specific simulated detector in 3. We then discuss the differences between different particles and how observables change as functions

of energy and angles in section 4 as well as mention systematics in section 5 before concluding in section 6.

2 Active Pixel Sensors

Nearly all semiconductor devices rely on using junctions of n- and p-type silicon to form diodes. Although bulk n- and p-type silicon are electrically neutral, n-type silicon has an excess of electrons in the conduction band while p-type silicon has an excess of holes in the valence band. When these two materials are joined together, thermal fluctuations lead to a diffusion of the excess charges to the region of opposite type. This creates an excess of negative charge in the p-type region and an excess of positive charge in the n-type region, creating an electric field between the two. The extent of this electric field determines the size of the *depletion region*.

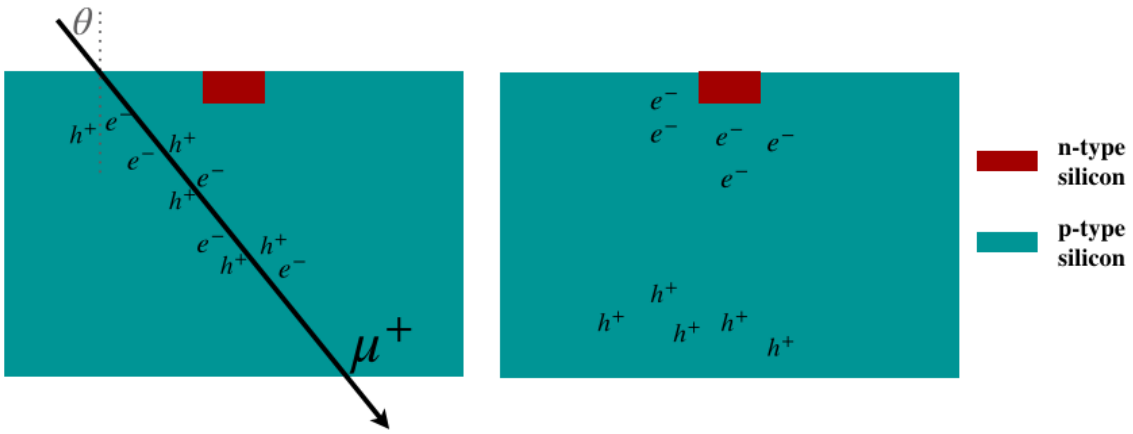

Figure 1. Schematic of an active pixel sensor (not drawn to scale). First, ionizing radiation enters the active region of the sensor (left) creating electron-hole pairs. Charges are then transported (right) because of the fields present from the diode formed by the junction, which can be digitized to produce a signal.

If ionizing radiation creates electron-hole pairs in the depletion region, then the electric fields will transport the charges, as shown in Figure 1. These charges can be gathered over a fixed integration time, and then digitized and read out as a signal.

Although most active pixel sensors used for astrophysical purposes use charge-coupled devices (CCDs), most cell phone image sensors are complementary metal-oxide sensors (CMOS). The difference is that CCDs, after an exposure, transport the charges deposited on each pixel to a common set of readout electronics. The charges are physically transported, and then read out systematically on the corner of a chip with many pixels [4]. CMOS detectors, on the other hand, places transistors directly in contact with each pixel, allowing to read out pixels individually. This distinction is not crucial for this simulation, but the underlying digitization of triggering a pixel based on charge deposited on each pixel is similar in logic to the CMOS implementation, which is what we would like to emulate. Additionally, in this framework, thresholds can be smeared out to reflect imperfections in read out electronics from pixel to pixel. This was not implemented in

this analysis, but would be an interesting investigation for future study, and may more accurately reflect physical detectors with imperfections.

A back of the envelope gives the rough number of electron-hole pairs that are created by a typical muon track. If the muon is minimum ionizing, then we can make the approximation that the energy loss is given by

$$\frac{dE}{dx} \approx \rho \left(2\,\mathrm{Me\,V cm^2/g}\right) \frac{Z^2}{\beta^2} \ . \tag{2.1}$$

Substituting the density of silicon ($\rho = 2.33\mathrm{g/cm^3}$), and assuming that the muon enters the detector with an angle of θ as defined in Figure 1, then the total energy deposited in the active region of the pixel is

$$E_{deposit} = 4.66 \cdot \frac{H}{\cos\theta} \qquad \text{(MeV)} \tag{2.2}$$

$$= \frac{12,256}{\cos\theta} \qquad \text{(eV)} \tag{2.3}$$

where H is the depletion thickness in cm, and we have substituted in the depletion thickness used in our simulation. In silicon, the energy required to create an electron-hole pair is 3.62 eV [5], which leads to a maximal number of electron-hole pairs created in the pixels of

$$N_{pair} \leq \frac{3386}{\cos\theta} \tag{2.4}$$

for minimum ionizing muons.

3 Allpix^2 Simulations

While rough estimates of electron-hole pairs can be calculated for minimum ionizing particles, the underlying particle interactions are stochastic in nature, and are most easily integrated using Monte Carlo techniques. We accomplish this using Allpix^2, a C++ open-source modular framework for the simulation of silicon pixel detectors [6] (code is available at [7]). Allpix^2 interfaces GEANT4 [8], a simulation toolkit which handles the particle interactions in matter, and requires a version of ROOT [9]. Modules can be selected to choose the type of silicon pixel, the dimensions of the pixel array, electric fields, charged particle transport, and digitization.

We simulate a pixel array similar to the one used in [3]. We ignore physical imperfections in the detector, though these could be the topic of a future study. We do model small electronics noise, but the magnitude of this noise does not lead to visible signatures in the final observables, and this could be changed to align more with the actual DECO dataset. The details of the physical geometry are included in Table 1, and an image of the detector interacting with a beam of muons is displayed in Figure 2.

We add additional, non-instrumented, silicon around the chip in order to reduce the amount of air around the detector. This allows us to recover some of the "worm" topologies [3] that result from numerous Coulomb scatters of energetic electrons within the detector volume.

For each simulation, we allow an integration time of 50ms to allow the electrons and holes to fully transport to the readout electronics. We also apply an electric field and bias voltage to aid

Table 1. Parameters of simulated device. Many parameters are chosen to mirror the analysis done in [3]. Some values are estimates as much of the information on the readout electronics in cell phone models is proprietary.

Parameter	Value
Number of Pixels	2592 × 1944 (5,038,848)
Pixel Size	0.9μm ×0.9μm
Depletion Thickness	26.3μm
Chip Thickness	10μm
Phone size	150mm × 70mm
Temperature	293K
Surrounding Material	Air

in the transport of the particles, though the magnitude of the actual fields in cell phones are not available. Because we do not know the exact threshold of pixels in the cell phones, we set a relaxed threshold of only needing 50 electrons to make it to the readout region of the pixel to register as a hit. The code is available at https://github.com/apizzuto/DECO_geant.

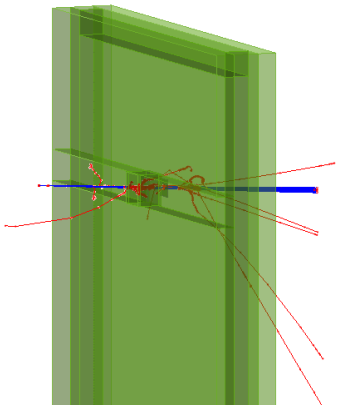

Figure 2. Simulation of a beam of 4GeV μ^+ (blue) interacting with the camera image sensor. The lens and screen are modeled as GEANT4 plexiglass and the remaining parts of the phone are modeled with aluminum. Negatively charged particles that are created from interactions are displayed in red.

4 Detector Distributions

Different particles can undergo different particle interactions in matter, and at different energies different cross sections dominate. These different cross sections ultimately lead to a different number of electron-hole pairs, and thus macroscopically different particle tracks.

4.1 Dependence on Incident Particle Type

First, we begin by simulating different beams of monochromatic photons at different energies as well as different incident angles. Photons below a few MeV are dominated by the cross section from the photoelectric effect, and these photons are unlikely to make it to the sensitive region of

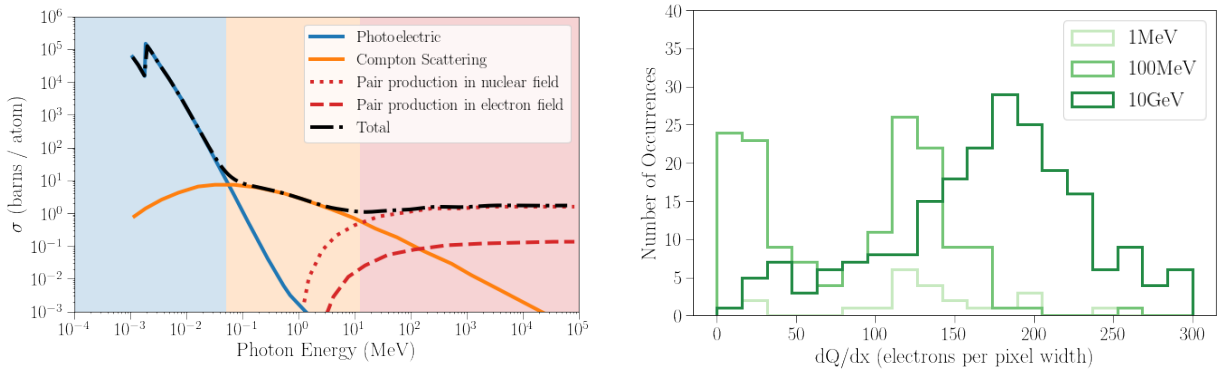

Figure 3. Photon cross sections (left) highlighting where each of the three relevant processes: photoelectric absorption, Compton scattering, and pair production, dominate (cross sections in Silicon from [10]). Photohadronic and other cross sections are included but are subdominant, for a complete description, see the GEANT4 Physics Lists documentation [8]. Total deposited charge for incident photons (right). Each energy had 1,000 photons simulated, the sums of the histograms are less than this because only a small fraction of incident photons interact in the silicon. The photons that do interact follow the expected pattern when compared to the total cross sections, but on average deposit less charge than muons of the same energy.

the detector, as the mean free path, λ, for photons of these energies is less than 1mm [5], and thus photons are photoabsorbed by parts of the cellphone external to the silicon pixels. However, at higher energies, photons reach the active region of the detector and interact, producing a detectable signature. Figure 3 shows distributions of deposited charge for 3 different energies. At low energies, most photons are photoabsorbed before reaching the detector. At the highest energies, the photons are likely to pair-produce, and the resulting electron-positron pair can be energetic enough to leave signals in the detector.

Next, we investigate the signatures of electrons in the detector. For both leptons we consider, at all energies, approximate energy losses are given by the Bethe-Bloch parameterization in [5],

$$\frac{dE}{dx} = \rho \frac{Z_{\text{nucl}}}{A_{\text{r}}} \left(0.307\text{MeVcm}^2/\text{g}\right) \frac{Z^2}{\beta^2} \left[\frac{1}{2} \ln\left(\frac{2m_e c^2 \beta^2 \gamma^2 T_{\text{max}}}{I^2}\right) - \beta^2 - \frac{\delta(\beta)}{2}\right] . \tag{4.1}$$

Other cross sections for energy losses are included in the simulation, but are subdominant compared to ionization losses. We inject 1,000 electrons at energies every half decade from 10keV to 10GeV. Incident angles are every 15 degrees with respect to the pixel normal, and from every incident particle, we extract the number of pixels that registered a hit, the charge on each of these pixels, and the locations of the pixels hit. With this information and knowledge of the geometry of the detector, we can extract information about the energy deposited per unit length, and this is displayed in Figure 4. For energies below about 10MeV, electrons do not reach the sensitive detector region, which explains the lack of events below this threshold in the figure.

To compare the charge deposited to energy lost per unit length, we assume the ionization losses transfer exactly the amount of energy required to create an electron-pair hole in silicon, 3.62eV. Above the threshold of around 10MeV for electrons, there is good agreement with the analytic result using this first order conversion between deposited charge and deposited energy, even though

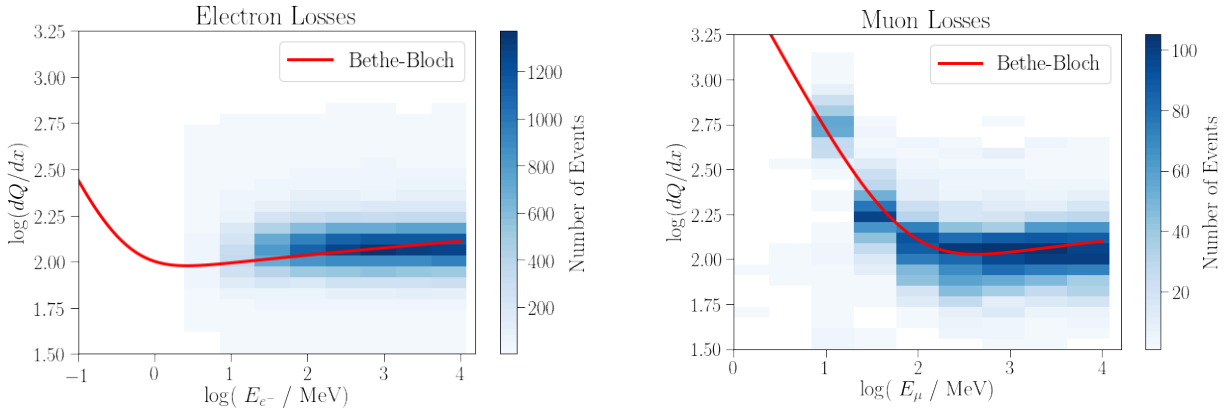

Figure 4. Simulations of incident electrons (left) and muons (right) as a function of incoming energy. Charge per length is in units of deposited electron charge per pixel width. The Bethe-Bloch line is obtained by taking Equation 4.1 and transforming from dE/dx to dQ/dx by multiplying by the energy required to liberate an electron charge in the sensitive region of the detector.

it neglects the additional energy that electrons gain from ionization that exceeds the threshold to create electron-hole pairs (energetic delta rays). Additionally, this assumption neglects the liberated charges that are not transported to pixels as well as the pixels that collect charges, but are below the threshold to trigger the digitization. Luckily, these two effects, neglecting energetic electrons and missing some pixels, are competing effects, which might help explain why our naive conversion results in good agreement with the model.

Finally, we consider the case of muons, again mainly discussing the interaction between the muons and the electrons in the silicon. For muons, below energies of around 100MeV, many muons interact or decay before reaching the sensitive detector volume, but at higher energies, muons become minimum ionizing particles (MIPs), losing approximately the same amount of energy per unit length. The comparison of expected minimum ionizing losses is also compared to the observed distributions in Figure 4, where again there is spread in each column due to the underlying stochastic nature of losses.

Characteristic event signatures for electrons, muons, and photons are included in Figure 5. Muons at most energies relevant to cosmic rays at sea level leave long track-like signatures in the detector. These could be used to reconstruct the initial direction of the muons. Electrons, depending on the energy, tend to undergo multiple scatters, and the deposition tends to be more stochastic, leading to occasional bright pixels followed by unhit pixels and then other large depositions offset from the original interaction region. Photons of the highest energies can pair produce and make leptons that leave visible signatures in the detector, while the lower energy photons tend to be photoabsorbed prior to entering the sensitive detector region.

4.2 Angular Dependence

With minimum ionizing muons, the track length holds the promise of providing a basis for per event reconstructions. The track length combined with the angle the track makes in the $x - y$ plane of

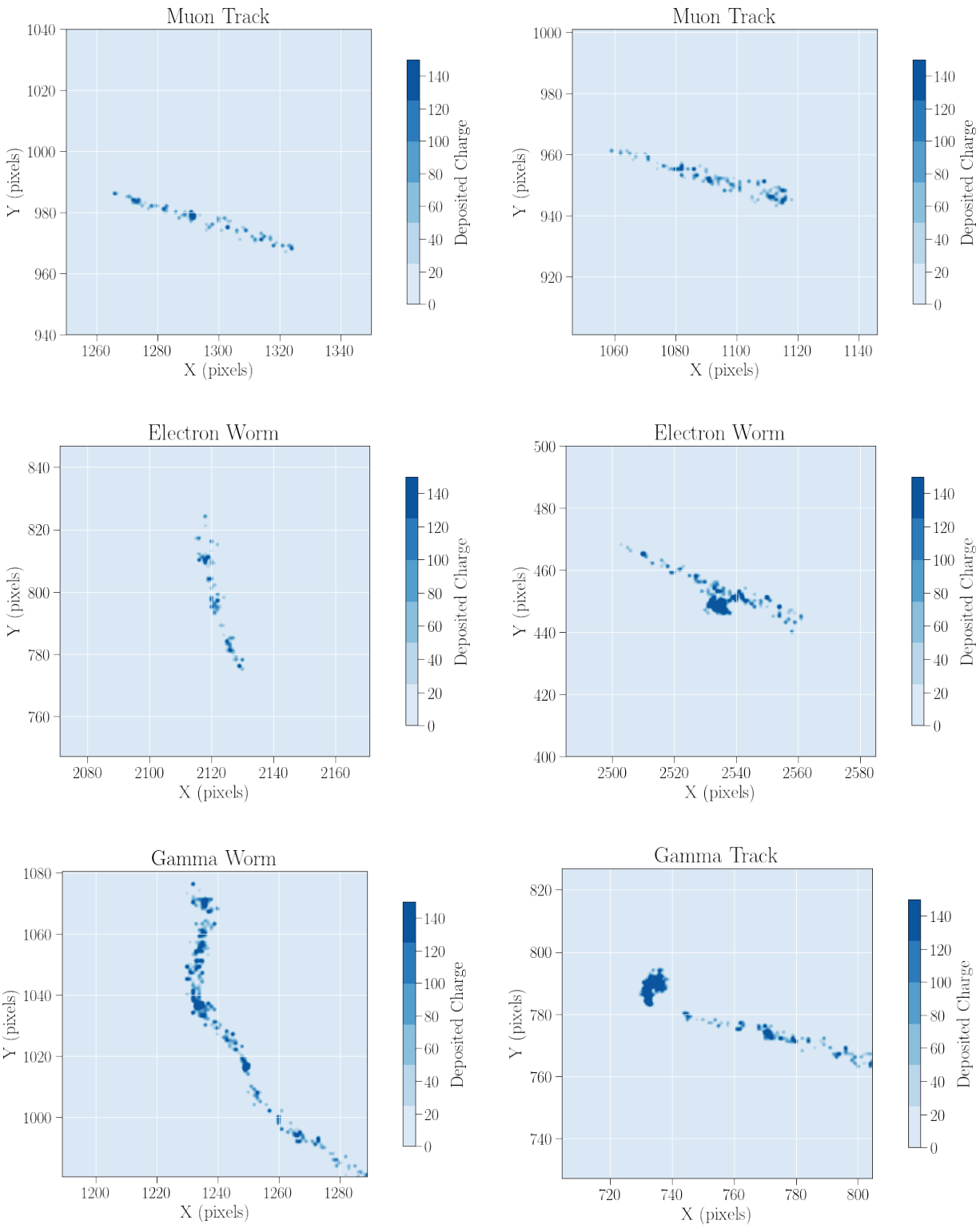

Figure 5. Typical event signatures for muons (top), electrons (middle), and gammas (bottom). Minimum ionizing muons leave long tracks in the detector, and are homogoneous over orders of magnitude in energy. Electrons tend to undergo multiple scatters, leaving signatures with more curvature, and occasionally undergo more catastrophic losses. Incident gammas leave different signatures depending on which interaction they undergo, which can either lead to "worm" like or "track" like morphologies.

the pixel array can be used to fix the incoming muon's zenith angle and azimuth with respect to the device, and metadata stored in data taking runs allow this to be mapped onto astronomical coordinate systems, such as celestial coordinates. However, there is still a degeneracy between antiparallel cosmic rays. To first order, one could assume that the cosmic rays are predominantly downgoing to remove this degeneracy, but differences between upgoing and downgoing tracks could be the topic of a future work.

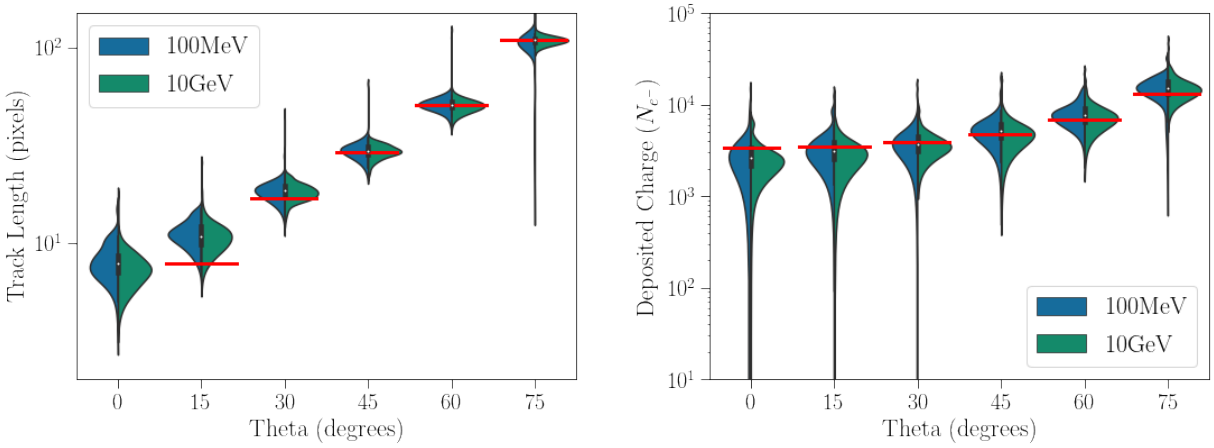

Figure 6. Dependence of observables on incident angle of muons. The plot on the left is a violin plot of observed track length as a function of incident angle with respect to the normal of the pixel array for two different benchmark energies. The right shows the total deposited charge as a function of the incident angle for muons of the same energies. Red shows the analytical approximation from the geometry of the detector with the assumption that the muons are MIPs.

If an incoming muon is minimum ionizing, and the threshold on the digitization is set appropriately, then the track length of a muon should be the exact projection of the trajectory onto the $x-y$ plane. However, although minimum ionizing losses are treated continuously, they are actually stochastic, and this stochastic nature as well as other interactions causes a spread in the observed track length for fixed incoming angles. Figure 6 displays the track length and deposited charge distributions for two benchmark energies covering the average range of energies of cosmic-ray muons at sea level. For minimum ionizing muons, although the energy of the incident muon might vary by orders of magnitude, the total deposited charge is centered around the same value, as is expected.

5 Systematics

All of the distributions shown above are for a fixed set of detector parameters, and reconstructions would rely on knowledge of the parameters. However, much of the information about the camera image sensors is proprietary. Here, we investigate the effect that modifying detector geometry has on detector signatures, as well as how electronics specifications cause the simulations to align better with the DECO dataset.

5.1 Depletion Thickness

Uncertainty on the size of the depletion thickness degrades the ability to reconstruct muons. Assume that a muon leaves a track in the detector of length l. If the depletion region is of height H, then the reconstructed angle, θ, is simply $\arctan(l/H)$. However, if there is an uncertainty on the depletion thickness, $H \to H + \delta$, then for this height the reconstructed angle, ϕ, goes as $\arctan(l/(H+\delta))$. The difference in these two measurements is then

$$\begin{aligned}\theta - \phi &= \arctan\frac{l}{H} - \arctan\frac{l}{H+\delta} \\ &= \arctan\left(\frac{\frac{\delta l}{H^2+\delta H}}{1-\frac{l^2}{H(\delta+H)}}\right) \\ &= \arctan\left(\frac{\delta l}{H(\delta+H)-l^2}\right),\end{aligned}$$

to first order in δ, and rewriting as an uncertainty, this gives us

$$\sigma_\theta \approx \frac{l}{H^2 - l^2} \times \sigma_H \tag{5.1}$$

Muon track lengths for different depletion thicknesses are given in Figure 7. The behavior scales as expected, with track length scaling as the projection of the muon track through the sensitive detector region onto the pixel plane. As there is a degeneracy for track length with respect to incident angle and depletion thickness, we display this systematic in the same way that we did for injecting events at different incident angles.

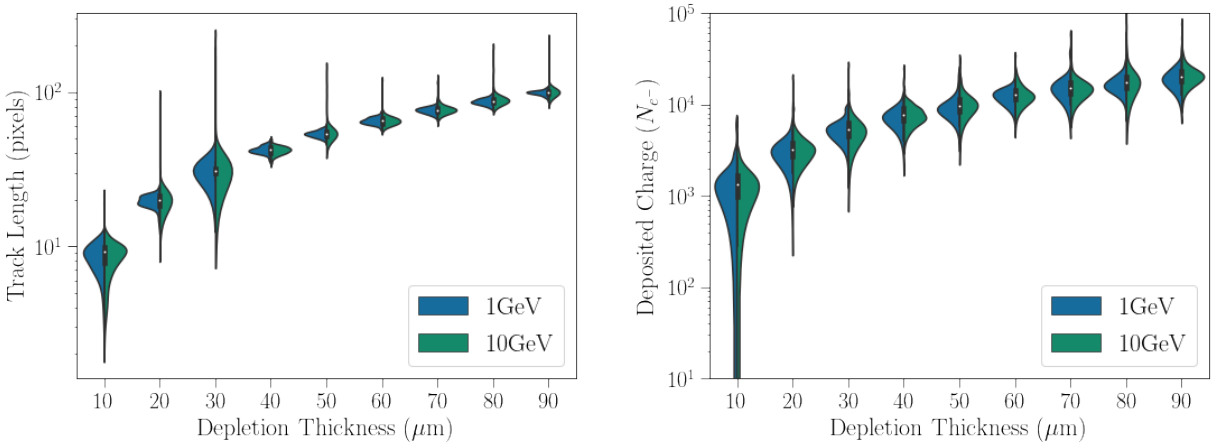

Figure 7. Dependence of observables on depletion thickness of the sensitive region. As expected, track length and deposited charge scale as the projection of the trajectory and length of the trajectory in the sensitive region, respectively.

5.2 Trigger Threshold

One immediate difference between the simulated event signatures and those present in the DECO dataset is that simulated muons have less continuous tracks than those on the database [1]. Here,

we investigate if that is due to the pixel threshold that was set in the simulations. The threshold to trigger a pixel was adjusted, and event images made for 1GeV muon tracks with an incident angle of 30 degrees with respect to the normal of the pixel plane, and images are displayed in Figure 8. The threshold has a notable effect on the continuity of the event signature, but even the smallest threshold is more disjoint than the actual events. This might be an indication of correlated electronics in the actual camera image sensors, which is not modeled in this analysis.

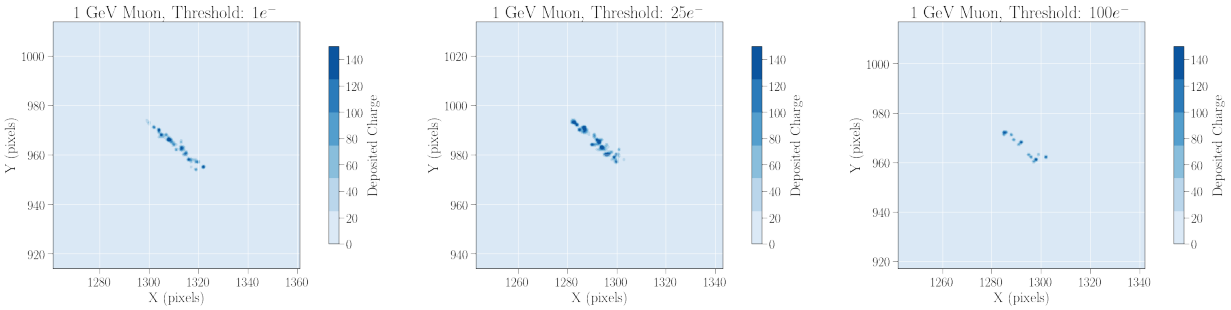

Figure 8. 1GeV Muon tracks for different trigger thresholds. Even for the smallest thresholds, muon tracks are more disjoint than in the actual DECO dataset.

6 Discussion & Conclusion

We have created a simulation software framework to reproduce images akin to those in the DECO dataset. Observables such as deposited charge and track length scale as they are expected to using known physics and geometrical arguments. Systematic and geometric uncertainties play a large role in being able to properly classify and reconstruct images in the DECO dataset, but with an understanding of these properties, this simulation lays the groundwork to make the first measurement of the cosmic-ray muon flux with cell phone camera image sensors.

Acknowledgments

This project was completed thanks to helpful discussion and planning with Rob Morgan. This simulation based analysis is meant as a complement to his direct irradiation measurements.

References

[1] DECO, "The Distributed Electronic Cosmic-ray Observatory." https://wipac.wisc.edu/deco/home.

[2] M. Winter, J. Bourbeau, S. Bravo, F. Campos, M. Meehan, J. Peacock, T. Ruggles, C. Schneider, A. L. Simons, and J. Vandenbroucke, *Particle Identification In Camera Image Sensors Using Computer Vision*, *Astropart. Phys.* **104** (2019) 42–53, [arXiv:1803.04493].

[3] J. Vandenbroucke et al., *Measurement of camera image sensor depletion thickness with cosmic rays*, *JINST* **11** (2016), no. 04 P04019, [arXiv:1511.00660].

[4] K. Bechtol, "Optical Astronomy Lecture." PHYS736 Lecture Notes.

[5] S. Tavernier, *Experimental Techniques in Nuclear and Particle Physics*. Springer, 2010.

[6] S. Spannagel, K. Wolters, D. Hynds, N. Alipour Tehrani, M. Benoit, D. Dannheim, N. Gauvin, A. NÃijrnberg, P. SchÃijtze, and M. Vicente Barreto Pinto, *Allpix^2: A Modular Simulation Framework for Silicon Detectors*, *Nucl. Instrum. Meth.* **A901** (2018) 164–172, [arXiv:1806.05813].

[7] K. Wolters et al., "Allpix Squared: Generic Pixel Detector Simulation Framework." https://project-allpix-squared.web.cern.ch/project-allpix-squared/.

[8] **GEANT4** Collaboration, S. Agostinelli et al., *GEANT4: A Simulation toolkit*, *Nucl. Instrum. Meth.* **A506** (2003) 250–303.

[9] R. Brun, *The development of the ROOT data analysis system*, *AIP Conf. Proc.* **583** (2001), no. 1 297.

[10] NIST, "PhysRefData." https://physics.nist.gov/PhysRefData/Xcom/html/xcom1.html.